ACS PHYSICAL CHEMISTRY Au
AN OPEN ACCESS JOURNAL OF THE AMERICAN CHEMICAL SOCIETY

pubs.acs.org/physchemau

Article

Extremely Fast Interfacial Li Ion Dynamics in Crystalline LiTFSI Combined with EMIM-TFSI

Bernhard Stanje and H. Martin R. Wilkening*

Cite This: *ACS Phys. Chem Au* 2022, 2, 136–142

Read Online

ACCESS | Metrics & More | Article Recommendations

ABSTRACT: Materials providing fast transport pathways for ionic charge carriers are at the heart of future all-solid state batteries that completely rely on sustainable, nonflammable solid electrolytes. The mobile ions in fast ion conductors may take benefit from structural disorder, cation and anion substitution, or dimensionality effects. While these effects concern the bulk regions of a given material, one may also manipulate the surface or interfacial regions of a polycrystalline poorly conducting electrolyte to enhance its transport properties. Here, we used ^{7}Li NMR to characterize interfacial effects in crystalline lithium bis(trifluoromethylsulfonyl)imide (LiTFSI) to which a small amount of ionic liquid EMIM-TFSI (EMIM: 1-ethyl-3-methylimidazolium cation, $C_6H_{11}N_2^+$) was added. We recorded longitudinal spin–lattice relaxation (SLR) curves $M_z(t_d)$ that directly mirror the ^{7}Li spin-fluctuations controlled by motional processes in such ionic-liquids-in-salt composites. Already at room temperature we observe strongly bimodal buildup curves $M_z(t_d)$ leading to two distinct SLR rates differing by a factor of 100. While the slower rate does exactly reflect the temperature behavior expected for poorly conducting LiTFSI, the faster rate mirrors rapid motional processes that are governed by an activation energy as low as 73 meV. We attribute these fast processes to highly mobile Li^+ ions in or near the contact area of crystalline LiTFSI and EMIM-TFSI. By using a method that characterizes motional processes from the atomic-scale point of view, we emphasize the importance of interfacial regions as reservoirs for fast Li^+ ions in such solid composite electrolytes.

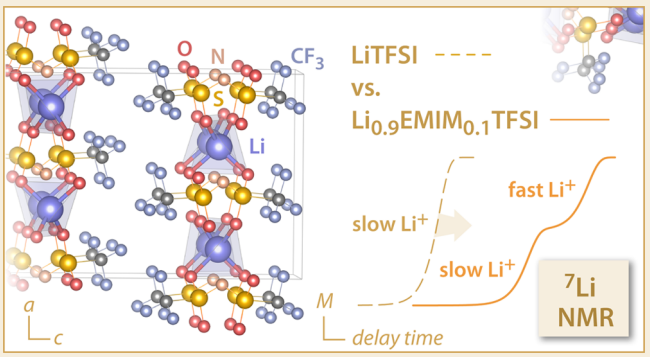

KEYWORDS: *ionic liquids, lithium, NMR, diffusion, transport, solid electrolytes*

1. INTRODUCTION

The feverish search for advanced materials acting as solid, temperature stable electrolytes in sustainable, electrochemical energy storage systems has reached an unprecedented level.[1,2] To date, we are still in the initial phase to understand and to identify the most important design strategies that lead to ultrafast ion dynamics in solids.[3] For instance, fast lithium-ion conductors may take advantage of substitutional effects, structural disorder, or low-dimensional transport pathways. Alternatively, one may generate a 3D network of interconnected interfacial pathways to guide the ions over macroscopic distances.[4,5] This concept is met in nanocrystalline materials that are equipped with a large volume fraction of, e.g., structurally disordered interfacial regions.[5,6] These regions, most likely also influenced by space charge effects,[7−11] provide fast through-going pathways for the single-charged ions.[12−15]

In so-called dispersed ion conductors, a Li-ion conducting phase is mixed on the nanometer length scale with a second compound that acts as insulating phase, such as Al_2O_3, TiO_2, or B_2O_3. Examples of such nanostructured composites[16] include LiI:Al_2O_3,[17] Li_2O:X_2O_3 (X = Al, B),[5,14,18−20] nano-confined $LiBH_4$:Al_2O_3,[21] LiF:Al_2O_3,[22] and LiF:TiO_2.[23]

As has been shown earlier,[24] poorly conducting LiTFSI (lithium bis(trifluoromethylsulfonyl)imide, LiX, X = TFSI ($N(CF_3SO_2)_2^-$)) can be turned into a highly conducting composite material by adding a small amount of an ionic liquid (IL) with the same anion, i.e., by adding EMIM-TFSI (EMIM means the 1-ethyl-3-methylimidazolium cation, $C_6H_{11}N_2^+$). $Li_{1-x}EMIN_xTFSI$ was termed "ionic-liquid-in-salt" electrolyte. It takes advantage of high (ionic) conductivities and an appreciable mechanical strength.[24] Furthermore, it can easily be supercooled to preserve high conductivities also at temperatures below ambient. Another exceptional advantage is the easy preparation of such compounds by combining the

Received: September 27, 2021
Revised: November 18, 2021
Accepted: November 19, 2021
Published: December 2, 2021

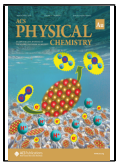

https://doi.org/10.1021/acsphyschemau.1c00032
ACS Phys. Chem Au 2022, 2, 136–142

salt LiX with different ionic liquids. Varying the composition of the IL-LiX compounds offers a rich playground to adjust the chemical and physical properties.

As yet, the exact origin of the significant enhancement seen for LiTFSI combined with EMIM-TFSI is still unknown. Commonly, the conduction properties of solid electrolytes are investigated by impedance spectroscopy being able to probe macroscopic ionic transport.[25] Less frequently, tracer diffusion experiments,[26] nuclear magnetic resonance,[27] muon spectroscopy,[28−30] and (quasi elastic) neutron scattering[31−33] or diffraction[26,34] are used to characterize ion dynamics in solids on different length scales and time scales. Here, we took advantage of time-domain ^{7}Li NMR spectroscopy[35,36] to directly probe the motional processes the Li spins are subjected to in a sample with the composition $(1-x)$LiTFSI:xEMIM-TFSI yielding $Li_{0.9}EMIN_{0.1}TFSI$ if $x = 0.1$ is chosen. Variable-temperature ^{7}Li NMR relaxation measurements[37] yield so-called magnetization transients that reflect the magnetic dipolar (and/or electric quadrupolar) fluctuations to which the spins are exposed. At sufficiently high temperatures, these fluctuations are driven by the motional processes taking place in the material under investigation.[35] Whereas in pure LiTFSI the spin−lattice relaxation transients follow single exponential time behavior, in $Li_{0.9}EMIN_{0.1}TFSI$ a pronounced two-component behavior is seen,[19] which we ascribe to the formation of highly conducting Li^+ diffusion pathways next to the untouched LiTFSI bulk regions. Our results emphasize the importance of interfacially generated transport pathways that we expect to play a crucial role in developing new solid electrolytes for, e.g., lithium-ion batteries.

2. EXPERIMENTAL SECTION

The $Li_{0.9}EMIN_{0.1}TFSI$ sample studied here was prepared according to the procedure described elsewhere; hence, we refer to the literature for details on the physical properties of the materials investigated in the present study. LiTFSI (Sigma-Aldrich, 99.9%) and EMIMTFSI (Solvionic, 99.9%) were dried under vacuum for 4 days. The materials were intimately mixed under intergas atmosphere (Ar gas) and then heated at 250 °C. After cooling to room temperature, the material was again mixed and heated for 30 min at 250 °C again. Crystalline $Li_{0.9}EMIN_{0.1}TFSI$ and LiTFSI were fire-sealed in glass ampules (4 mm in diameter, 2 cm in length) to protect the material permanently from any reaction with moisture and air. We employed a Bruker 500 MHz NMR spectrometer connected to an 11 T magnet to record ^{7}Li (spin quantum number $I = 3/2$) NMR spin−lattice relaxation transients as a function of temperature T. The sample chamber of the standard Bruker probe was continuously flushed with a stream of heated nitrogen to adjust the temperature which was regulated with a Eurotherm temperature controller. We used a Ni-CrNi thermocouple to measure the temperature near the sample; calibration of the thermocouple leads to an average error margin of ±2 K.

These magnetization transients were recorded with the saturation recovery pulse sequence,[38] where a train of ten 90° pulses (2 μs (nonselective) pulse length, 150 W power), spaced by 80 μs, destroys any longitudinal magnetization M_z. The saturating recovery pulse sequence does not need long recycle delays. Its recovery due to spin-fluctuations mediated or controlled by motional processes of the Li ions is then recorded as a function of a sufficiently long delay time t_d with a 90° detection pulse. Only long t_d times, with values of up to 1000 s, guaranteed the full recovery of longitudinal magnetization. Usually, we used up to eight scans per waiting time t_d and plotted the area of the accumulated free inductions decay (FID) as a function of t_d. The buildup curves were parametrized with exponential functions, $M_z(t_d) \propto \exp(-t_d/T_1)$. While for pure LiTFSI a single exponential is enough to reproduce the curve, for the composite $Li_{0.9}EMIN_{0.1}TFSI$, in contrast, a biexponential recovery was observed[13,19] and, thus, we used a sum of two exponentials to analyze the overall response. Hence, in the case of $Li_{0.9}EMIN_{0.1}TFSI$, a single T_1 experiment leads to two ^{7}Li NMR spin−lattice relaxation rates, $1/T_{1,slow}$ and $1/T_{1,fast}$, which individually depend on temperature T. The ^{7}Li NMR spectra, that is, the quadrupole powder patterns, were analyzed with DMFit software to estimate the quadrupole coupling constants C_q and the asymmetry parameter η, ranging from 0 (axial symmetry) to 1. ^{7}Li NMR spectra were obtained directly from the FIDs of the SLR measurements through Fourier transformation; the spectra refer to the longest waiting times t_d.

3. RESULTS AND DISCUSSION

To characterize the structural and dynamic situation in $Li_{0.9}EMIN_{0.1}TFSI$, we first recorded ^{7}Li NMR spectra. These spectra were already presented and discussed in detail in an earlier study[24] that introduced the liquid-in-salt LiTFSI-EMIMTFSI system. Here, we briefly repeat the main characteristics seen in ^{7}Li NMR. For this purpose, in Figure 1, the evolution of the ^{7}Li NMR spectra with increasing temperature is shown. At low T, the line is composed of a central intensity and a quadrupole powder pattern that is

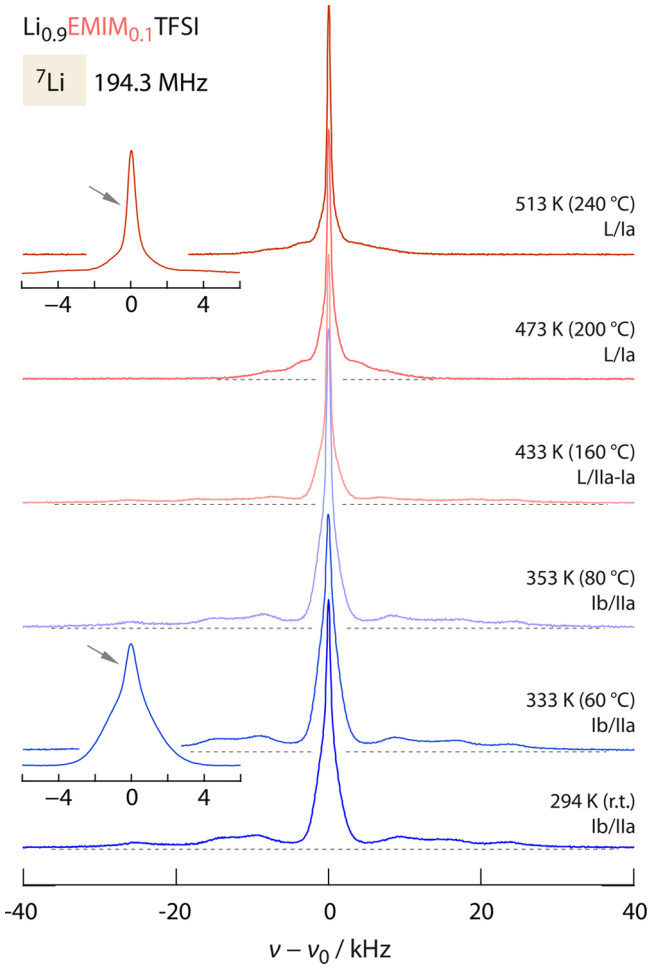

Figure 1. ^{7}Li NMR spectra of $Li_{0.9}EMIN_{0.1}TFSI$ recorded at the temperatures indicated. Spectra were acquired under nonrotating, i.e., static conditions. They reveal a two-component central line (magnetic spin quantum number $m_I = 1/2 \rightleftarrows -1/2$) which consists of a broad component and a motionally narrowed line as is best seen in the two insets included. Arrows point to the motionally averaged NMR line whose area fraction increases with temperature. Data were taken from our previous publication.[24]

https://doi.org/10.1021/acsphyschemau.1c00032
ACS Phys. Chem Au 2022, 2, 136−142

identical with that of pure, crystalline LiTFSI (phase IIa). The pattern slightly changes when the crystalline EMIM-TFSI phase (Ib) starts to melt, indicated by the label L. The second, rather obvious, change of the pattern occurs at higher T (ca. 150 °C),[24] when LiTFSI undergoes a solid−solid phase transformation (IIa ⇄ Ia), which is also documented in literature.[39] These changes are best seen in Figure 2,

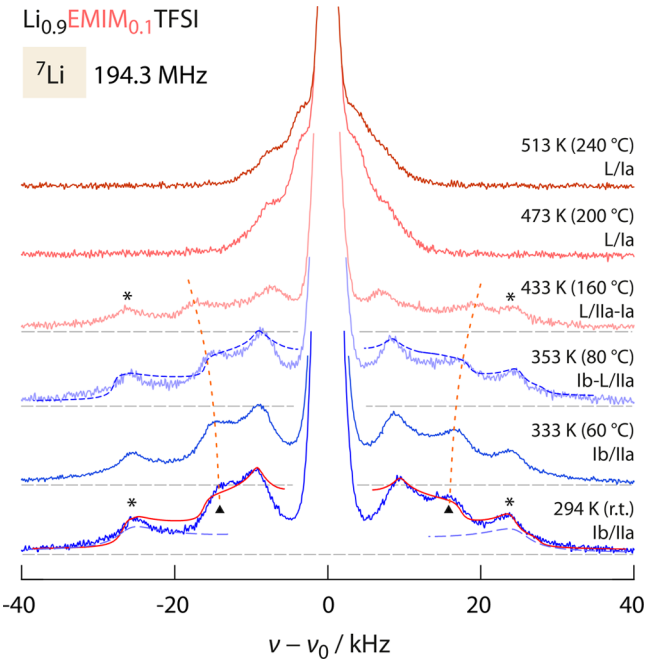

Figure 2. Magnification of the ^{7}Li NMR spectra of $Li_{0.9}EMIN_{0.1}TFSI$ shown in Figure 1. The pattern here shows the change in quadrupole intensities as a function of temperature. Dashed and solid lines (see the spectra recorded at 294 and 353 K) show a simulation of the whole pattern assuming two electrically inequivalent Li sites. See the text for further details.

presenting a magnification of the ^{7}Li NMR quadrupole patterns. The changes Ib-L and IIa-Ia do perfectly agree with results from differential scanning calorimetry published earlier.[24]

Here, we simulated the quadrupole intensities of the NMR line recorded at 294 K assuming two sets of electrically inequivalent Li sites for which the quadrupole moment of the Li spin is each subjected to a distinct electric field gradient. We also tried to simulate the spectrum with a single set of parameters as the LiTFSI structure if analyzed by X-ray diffraction suggest only one crystallographical Li site.[40] Such a simulation (η = 0.27, C_q = 27 kHz) does less satisfactorily reproduce the full spectrum. The simulation is shown in Figure 2 using solid (294 K) and dashed lines (353 K), respectively. The dashed line plotted together with the spectrum recorded at 294 K represents the outer quadrupole intensities pointing to an axially symmetric EFG characterized by a coupling constant C_q of 52 kHz, see the 90° singularities marked with asterisks. This pattern does not change much with temperature until 160 °C. Instead the inner satellite pattern, leading to η = 0.28, C_q = 27 kHz, depends slightly on temperature (see the curved, dashed lines drawn); presumably, also other solid−solid transitions may affect its shape.[41] This pattern, whose outer singularities are marked by triangles in Figure 2, changes when the Ib phase starts to melt; another drastic change is seen when LiTFSI undergoes the solid−solid phase transition,[39] as mentioned above. We have to note that also slight chemical shift anisotropies affect the patterns seen in Figure 2. Our results suggest that the local Li coordination in LiTFSI seems to be more complex than originally assumed in the literature; a detailed structural study is, however, beyond the scope of the present study. The evolution of the quadrupole pattern gets even more complex as motion-induced averaging processes contribute to the changes seen in Figure 2; finally, a pattern characterized by a largely reduced coupling constant is obtained at 473 K, that is, well above the IIa-Ia phase transition.

Most important for the dynamic study here, is, however, the motion-controlled change of the ^{7}Li NMR central transition. The central line of $Li_{0.9}EMIN_{0.1}TFSI$ clearly reveals a dynamically heterogeneous spin system, which already becomes apparent when we consider the ^{7}Li NMR central transition recorded at 294 K. In contrast to the NMR central line belonging to the ^{7}Li NMR spectrum of crystalline LiTFSI, the one of $Li_{0.9}EMIN_{0.1}TFSI$ is composed of *two* contributions, that is, a motionally narrowed line superimposes the broad line being characteristic for LiTFSI as is shown in the insets of Figure 1. We attribute this narrowed line to a ^{7}Li subensemble that is subjected to rapid spin fluctuations, i.e., to rapid motional processes.[5] Obviously, these dynamic processes are able to average the dipole−dipole interactions being responsible for line broadening occurring in solid-state NMR at low temperatures.

With raising temperature, the area fraction under the narrow line increases revealing that also the number of Li^+ ions taking part in this fast diffusion process increases, see the line recorded at 513 K. To put it in a nutshell, the ^{7}Li NMR central lines reveal two dynamically different spin ensembles in $Li_{0.9}EMIN_{0.1}TFSI$. In contrast, in crystalline LiTFSI only the less mobile ions, represented by the dipolarly broadened central line, are visible by NMR. Hence, we assign the fast diffusing spins to those ^{7}Li ions that benefit from the LiTFSI| EMIM-TFSI interfacial regions in the composite with the overall composition $Li_{0.9}EMIN_{0.1}TFSI$. This assignment is in agreement with earlier studies focusing on similar (nanocrystalline or nanoconfined) two-phase systems.[13,16,21,22,42]

To quantify the dynamic properties the two spin ensembles, we recorded ^{7}Li NMR spin−lattice relaxation transients $M_z(t_d)$ and studied their evolution as a function of temperature T, see Figure 3. We assume that magnetization recovery is most likely induced by both magnetic dipolar and to a larger extent by electric quadrupolar interactions. ^{6}Li NMR SLR rate measurements would give further insights. In the half-logarithmic plot of Figure 3a the ^{7}Li NMR transients $M_z(t_d)$ of crystalline LiTFSI are shown that were recorded at three different temperatures (60 °C, 120 °C, 200 °C). Dashed lines show fits with single exponential functions. The corresponding temperature-dependent ^{7}Li NMR spin−lattice rates are included in the Arrhenius diagram of Figure 4. They agree with the rate $1/T_{1,slow}$ which can be extracted from the biexponential transients of the LiTFSI-EMIMTFSI composite. These transients are displayed in Figure 3b.

Especially at low temperatures the transients of the composite reveal a pronounced two-step buildup behavior when coming from short waiting times t_d (see Figure 3b). The first buildup step mirrors rapid spin-fluctuations described by the rate $1/T_{1,fast}$, corresponding to the narrow component of the associated ^{7}Li NMR spectra. The second increase in

https://doi.org/10.1021/acsphyschemau.1c00032
ACS Phys. Chem Au 2022, 2, 136−142

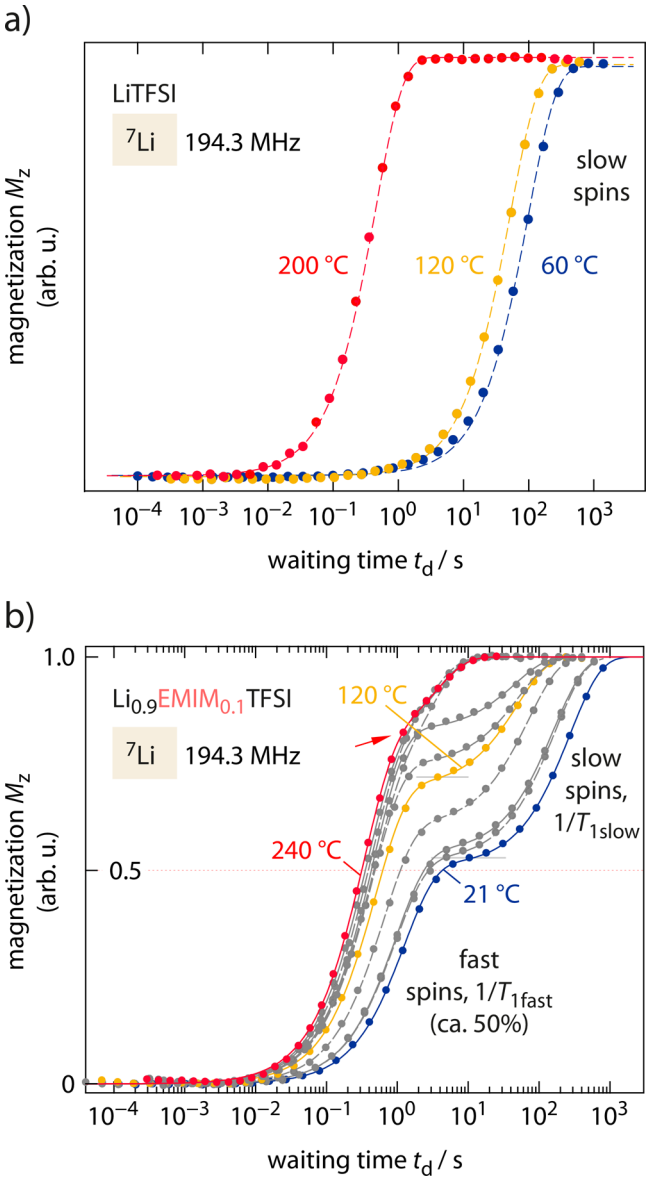

Figure 3. (a) ^{7}Li NMR spin−lattice relaxation transients (194.3 MHz) of crystalline LiTFSI, recorded at the temperatures indicated. The shape of the transients follows that of ideal exponential functions and does not change with temperature. (b) ^{7}Li NMR spin−lattice relaxation transients of LiTFSI-EMIMTFSI. The two-step buildup curves lead to two rates $1/T_{1,fast}(1/T)$ and $1/T_{1,slow}(1/T)$ that differently depend on temperature. The rate $1/T_{1,slow}$ equals that which governs ^{7}Li NMR spin−lattice relaxation in crystalline LiTFSI.

$M_z(t_d)$, which is seen at longer waiting times and which leads to the saturation magnetization $M_z(\infty)$, is characterized by the rate $1/T_{1,slow}$. Although less pronounced, even at temperatures as high as 240 °C, the two-step behavior of the transients is clearly seen, cf. the arrow in Figure 3b pointing to the deviation of the curve from single exponential behavior at longer waiting times. The change in amplitude of the two parts of the overall magnetization transients reveals that the number of fast Li spins increases with temperature. It is ca. 50% at room temperature and reaches ca. 80% at 240 °C. This behavior is fully consistent with that which is seen in NMR line shape measurements. The motionally narrowed ^{7}Li NMR line grows at the expense of the broader line; see Figure 1.[24] The same behavior has also been observed for other single-phase nanocrystalline materials that show fast dynamics of the ions located in their interfacial regions.[42]

Since for ideal single exponential buildup curves the spin−lattice relaxation time T_1 corresponds to the waiting time t_d at which the curve passes through its inflection point, we recognize that the two components of the overall transients show quite different temperature behaviors. The component characterizing the fast spin reservoir, leading to $1/T_{1,fast}$, depends weaker on temperature than the component representing the slow spins in crystalline LiTFSI. The change of the two rates $1/T_{1,fast}$ and $1/T_{1,slow}$ with the inverse temperature $1/T$ is shown in Figure 4.

At low T, $\log_{10}(1/T_{1,slow}(1/T))$ vs $1/T$ reveals a linear regime whose slope yields an activation energy E_a of 0.2 eV and characterizes (local) magnetic-dipolar and/or electric quadrupolar spin-fluctuations the ^{7}Li spins in LiTFSI are sensing. In general, we assume $1/T_1(1/T)$ follows Arrhenius behavior and that the jump rate $1/\tau$, to which $1/T_1$ is proportional, is given by $1/\tau = 1/\tau_0 \exp(-E_a/(k_B T))$; k_B denotes Boltzmann's constant, and $1/\tau_0$ is the pre-exponential factor. For comparison, impedance spectroscopy yielded 0.25 eV in the temperature from 80 to 130 °C (see Figure 3),[24] which is in quite good agreement even if we take into account that NMR is more sensitive to local jump processes than long-range ion transport in this T range. At $T \approx 80$ °C, the NMR rates $1/T_{1,slow}$ pass into an almost temperature independent regime mirroring the effect of melting of the EMIM-TFSI phase in the composite. This feature, which is fully reversible upon heating or cooling, is also seen in ^{7}Li NMR spectra presented in Figure 2. Most likely, the rates in this regime are influenced by effective spin-diffusion effects driven by both Li^+ translational motions as well as by rotational (or translational) motions of the complex anions. Whether this kink is also seen in pure LiTFSI is still unclear as we have not analyzed the full temperature range. If also appearing in pure LiTFSI, it might be due a change of the local coordination of Li^+ in LiTFSI; indeed, the phase diagram in literature points to such phenomena.[41]

Finally, at even higher temperatures, the solid−solid phase transitions of LiTFSI cause the rates of $1/T_{1,slow}$ to abruptly increase. The behavior of $1/T_{1,slow}$ resembles that of crystalline LiTFSI without any EMIM-TFSI; thus, $1/T_{1,slow}$ is governed by the spin fluctuations to which the ions in the LiTFSI regions are subjected.

In stark contrast to $1/T_{1,slow}$, the rate $1/T_{1,fast}$, which can exclusively be probed for the LiTFSI-EMIMTFSI system, shows a completely different temperature behavior that is affected neither by the melting of the EMIM-TFSI phase nor by the solid−solid phase transitions. Obviously, the two spin-systems in LiTFSI-EMIMTFSI are spatially and energetically decoupled from each other. Here, we assign the spin-ensemble characterized by $1/T_{1,fast}$ to those spins being located in or near the interfacial regions of the supercooled LiTFSI|EMIM-TFSI composite. Such an assignment would be in agreement with nanocrystalline and nanoconfined systems studied earlier by NMR; see above.[13,16,19,21] These regions, as has been shown for nanocrystalline ceramics, are extended over a region of 2−4 nm.[42] In the present case, Li^+ ion dynamics of this fast spin ensemble is characterized by a very low activation energy as low as 73 meV. Such a value is even lower by more than a factor of 2 than that which has recently been probed for Li^+ ion dynamics in the interfacial regions of nanocrystalline $LiBH_4$ (180 meV).[13] It definitely reveals extremely fast Li^+ ion

https://doi.org/10.1021/acsphyschemau.1c00032
ACS Phys. Chem Au 2022, 2, 136−142

exchange processes in the LiTFSI|EMIM-TFSI composite studied here.

In a previous work,[43] Matsumoto et al. reported on the coordination environment around the lithium cation in solid $Li_2(EMIM)(N(SO_2CF_3)_2)_3$. In this compound, which might be formed as a thin layer on the interfacial regions of our LiTFSI crystallites, two crystallographically inequivalent lithium sites are present; the Li ions are trigonal-bipyramidally coordinated by five oxygen atoms of the $N(SO_2CF_3)_2$ anions forming a two-dimensional network. One might speculate whether Li^+ ion dynamics in such a 2D network is at the origin of the rather fast Li^+ spin fluctuations seen in our experiment.

The value of 73 meV has to be interpreted as a mean activation energy that describes the elementary Li^+ hopping processes on the angstrom length scale. In contrast to NMR, conductivity measurements, precisely speaking conductivity values measured in the direct current limit of broadband conductivity spectroscopy, are able to probe long-range ion transport. Hence, we expect the activation energies from conductivity spectroscopy to be larger than those measured by NMR. Indeed, in $Li_{0.9}EMIN_{0.1}TFSI$, the activation energies turned out to be 0.25 eV (80−130 °C) and 0.42 eV (150−180 °C) if we analyze the impedance data (see Figure 4), which were taken from an earlier study.[24] The specific ionic conductivity reaches a value of ca. 1 mS cm^{-1} at 450 K.[24] This temperature is well above the melting point of the EMIM-TFSI phase. Below 348 K (75 °C), that is, when entering the crystalline Ib/IIa regime the conductivity of $Li_{0.9}EMIN_{0.1}TFSI$ sharply decreases until at room temperature it takes a value of only 10^{-11} S cm^{-1}.[24] Whereas conductivity measurements tell us that long-range ion transport is extremely poor in this crystalline regime of the LiTFSI|EMIM-TFSI composites,[24] NMR reveals, however, rapid Li^+ movements on a local length scale even at ambient conditions; see the two-component NMR central lines in combination with the distinctive two-step relaxation curves recorded at 294 K. These local exchange processes do, however, not lead to an enhancement in long-range ion transport at ambient conditions. Increasing the amount of EMIM-TFSI clearly leads to an increase in long-range ion transport, as has been reported earlier.[24] We think that this increase is strongly related to the interfacial ion dynamics probed here for $Li_{0.9}EMIN_{0.1}TFSI$.

4. CONCLUSION

To conclude, extremely fast spin dynamics has been found in composites composed of crystalline LiTFSI and EMIM-TFSI containing only a small volume fraction of the latter compound. ^{7}Li NMR spectra, which were recorded as a function of temperature, revealed a subset of Li ions which perform rapid movements being sufficient to average homonuclear dipole−dipole interactions. The corresponding ^{7}Li NMR magnetization transients, which we recorded in the frame of classical saturation recovery experiments, are composed of two dynamically distinct spin ensembles. While the slower spins show the same relaxation behavior as those in pure LiTFSI, the fast ensemble is attributed to those spins that benefit from the LiTFSI|EMIM-TFSI interfacial regions formed, possibly also involving the formation of a second phase covering these regions. The extremely low activation energy of only 0.073 eV points to a very flat potential landscape. The fact that the diffusion-induced $1/T_1$ NMR rate peak is not seen until 500 K reveals that the underlying Arrhenius behavior has to be described by a rather low pre-exponential factor $1/\tau_0$ also determining the overall Li^+ jump rate $1/\tau$.

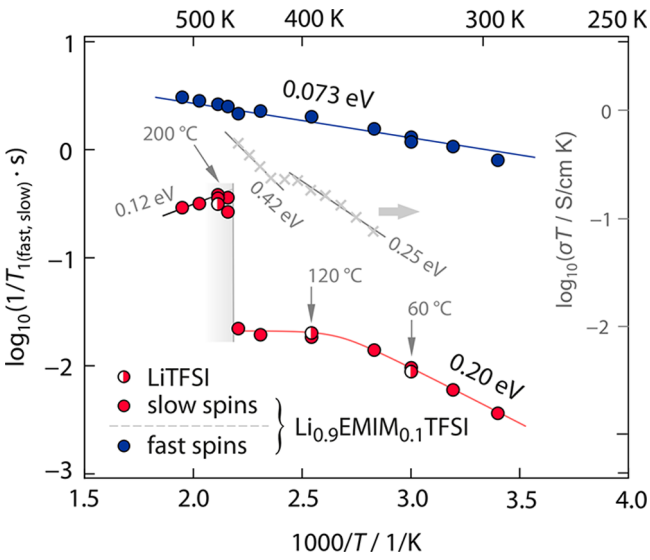

Figure 4. Arrhenius plot of the rates $1/T_{1,slow}$ and $1/T_{1,fast}$ that determine heterogeneous ^{7}Li NMR spin−lattice relaxation in the LiTFSI-EMIMTFSI system ($Li_{0.9}EMIN_{0.1}TFSI$). The rates are obtained from a single T_1 experiment. Those of crystalline LiTFSI, here exemplarily shown for three different temperatures (60, 120 and 200 °C), coincide with the magnetization component that represents the ensemble of slow spins in LiTFSI-EMIMTFSI. The solid−solid phase transition causes the rate $1/T_{1,slow}$ to sharply increase at ca. 180 °C. It does not affect the rate $1/T_{1,fast}$ following Arrhenius behavior that is characterized by an activation energy E_a as low as 73 meV. We assume that $1/T_{1,fast}$ is mainly driven by the highly mobile Li^+ ions near the LiTFSI|EMIMTFSI interfacial regions. Error bars are smaller than the symbol size. For comparison, the change of the ionic conductivity σ, plotted as $\log_{10}(\sigma T)$ vs $1/T$, is also shown; see the right axis. See the text for further explanation.

Our results reveal the importance of interfacial regions in materials suitable to act as solid electrolytes in future energy storage systems such as Li-based batteries. Designing and taking benefit from such regions offers another degree of freedom to manipulate ion dynamics in solids. In many cases, enhanced Li ion dynamics in such regions is influenced by local site disorder or by extended space charge regions that govern transport properties in nanostructured artificial ion conductors. Only in few cases the separate study of these highly mobile charge carriers has been shown. The present study illustrates once more the usefulness of classical charge-carrier specific NMR experiments to characterize heterogeneous dynamics in complex solids.

AUTHOR INFORMATION

Corresponding Author

H. Martin R. Wilkening − *Institute of Chemistry and Technology of Materials (NAWI Graz), Graz University of Technology, A-8010 Graz, Austria;* orcid.org/0000-0001-9706-4892; Email: wilkening@tugraz.at

Author

Bernhard Stanje − *Institute of Chemistry and Technology of Materials (NAWI Graz), Graz University of Technology, A-8010 Graz, Austria*

Complete contact information is available at:

https://doi.org/10.1021/acsphyschemau.1c00032
ACS Phys. Chem Au 2022, 2, 136−142

https://pubs.acs.org/10.1021/acsphyschemau.1c00032

Notes

The authors declare no competing financial interest.

■ ACKNOWLEDGMENTS

We thank the group of P. Johansson (Chalmers, Sweden) for giving us the opportunity to record NMR spectra on a previous series of samples, which encouraged us to prepare our own $Li_{0.9}EMIN_{0.1}TFSI$ sample and to carry out long-time NMR spin−lattice relaxation measurements, see Figure 3. Financial support by the German Science Foundation (DFG, Grant No. WI3600, 4-1) in the frame of the former Research Unit (Forschungsgruppe molife) 1277 is gratefully acknowledged.

■ REFERENCES

(1) Zhang, Z. Z.; Shao, Y. J.; Lotsch, B.; Hu, Y. S.; Li, H.; Janek, J.; Nazar, L. F.; Nan, C. W.; Maier, J.; Armand, M.; et al. New Horizons for Inorganic Solid State Ion Conductors. *Energy Environ. Sci.* **2018**, *11*, 1945−1976.

(2) Bachman, J. C.; Muy, S.; Grimaud, A.; Chang, H. H.; Pour, N.; Lux, S. F.; Paschos, O.; Maglia, F.; Lupart, S.; Lamp, P.; et al. Inorganic Solid-State Electrolytes for Lithium Batteries: Mechanisms and Properties Governing Ion Conduction. *Chem. Rev.* **2016**, *116*, 140−162.

(3) Ohno, S.; Banik, A.; Dewald, G. F.; Kraft, M. A.; Krauskopf, T.; Minafra, N.; Till, P.; Weiss, M.; Zeier, W. G. Materials Design of Ionic Conductors for Solid State Batteries. *Progr. Energy* **2020**, *2*, 022001.

(4) Knauth, P. Inorganic Solid Li ion Conductors: An Overview. *Solid State Ionics* **2009**, *180*, 911−916.

(5) Heitjans, P.; Indris, S. Diffusion and Ionic Conduction in Nanocrystalline Ceramics. *J. Phys.: Condens. Matter* **2003**, *15*, R1257−R1289.

(6) Heitjans, P.; Wilkening, M. Ion dynamics at interfaces: nuclear magnetic resonance studies. *MRS Bull.* **2009**, *34*, 915−922.

(7) Maier, J. Ionic Conduction in Space Charge Regions. *Prog. Solid State Chem.* **1995**, *23*, 171−263.

(8) Sata, N.; Eberman, K.; Eberl, K.; Maier, J. Mesoscopic Fast Ion Conduction in Nanometre-Scale Planar Heterostructures. *Nature* **2000**, *408*, 946−949.

(9) Maier, J. Nano-Ionics: Trivial and Non-Trivial Size Effects on Ion Conduction in Solids. *Z. Phys. Chem.* **2003**, *217*, 415−436.

(10) Maier, J. Nanoionics: Ion Transport and Electrochemical Storage in Confined Systems. *Nat. Mater.* **2005**, *4*, 805−815.

(11) Maier, J. Nanoionics: Ionic Charge Carriers in Small Systems. *Phys. Chem. Chem. Phys.* **2009**, *11*, 3011−3022.

(12) Prutsch, D.; Breuer, S.; Uitz, M.; Bottke, P.; Langer, J.; Lunghammer, S.; Philipp, M.; Posch, P.; Pregartner, V.; Stanje, B.; et al. Nanostructured Ceramics: Ionic Transport and Electrochemical Activity A Short Journey Across Various Families of Materials. *Z. Phys. Chem.* **2017**, *231*, 1361−1405.

(13) Breuer, S.; Uitz, M.; Wilkening, H. M. R. Rapid Li Ion Dynamics in the Interfacial Regions of Nanocrystalline Solids. *J. Phys. Chem. Lett.* **2018**, *9*, 2093−2097.

(14) Indris, S.; Heitjans, P.; Roman, H. E.; Bunde, A. Nanocrystalline versus Microcrystalline $Li_2O:B_2O_3$ Composites: Anomalous Ionic Conductivities and Percolation Theory. *Phys. Rev. Lett.* **2000**, *84*, 2889−2892.

(15) Puin, W.; Rodewald, S.; Ramlau, R.; Heitjans, P.; Maier, J. Local and Overall Ionic Conductivity in Nanocrystalline CaF_2. *Solid State Ionics* **2000**, *131*, 159−164.

(16) Heitjans, P.; Wilkening, M. Ion Dynamics at Interfaces: Nuclear Magnetic Resonance Studies. *MRS Bull.* **2009**, *34*, 915−922.

(17) Liang, C. C. Conduction Characersitics of Lithium Iodide Aluminium Oxide Solid Electrolytes. *J. Electrochem. Soc.* **1973**, *120*, 1289−1292.

(18) Indris, S.; Heitjans, P. Heterogeneous ^{7}Li NMR Relaxation in Nanocrystalline $Li_2O:B_2O_3$ Composites. *J. Non-Cryst. Solids* **2002**, *307*, 555−564.

(19) Wilkening, M.; Indris, S.; Heitjans, P. Heterogeneous Lithium Diffusion in Nanocrystalline Li_2O Al_2O_3 Composites. *Phys. Chem. Chem. Phys.* **2003**, *5*, 2225−2231.

(20) Indris, S.; Heitjans, P.; Ulrich, M.; Bunde, A. AC and DC Conductivity in Nano- and Microcrystalline $Li_2O:B_2O_3$ Composites: Experimental Results and Theoretical Models. *Z. Phys. Chem.* **2005**, *219*, 89−103.

(21) Zettl, R.; Hogrefe, K.; Gadermaier, B.; Hanzu, I.; Ngene, P.; De Jongh, P. E.; Wilkening, H. M. R. Conductor-Insulator Interfaces in Solid Electrolytes: A Design Strategy to Enhance Li-Ion Dynamics in Nanoconfined $LiBH_4/Al_2O_3$. *J. Phys. Chem. C* **2021**, *125*, 15052−15060.

(22) Breuer, S.; Pregartner, V.; Lunghammer, S.; Wilkening, H. M. R. Dispersed Solid Conductors: Fast Interfacial Li-Ion Dynamics in Nanostructured LiF and LiF:γ-Al_2O_3 Composites. *J. Phys. Chem. C* **2019**, *123*, 5222−5230.

(23) Gombotz, M.; Pree, K. P.; Pregartner, V.; Hanzu, I.; Gadermaier, B.; Hogrefe, K.; Wilkening, H. M. R. Insulator:conductor Interfacial Regions — Li Ion Dynamics in the Nanocrystalline Dispersed Ionic Conductor LiF:TiO_2. *Solid State Ionics* **2021**, *369*, 115726.

(24) Marczewski, M. J.; Stanje, B.; Hanzu, I.; Wilkening, M.; Johansson, P. "Ionic liquids-in-Salt" - a Promising Electrolyte Concept for High-Temperature Lithium Batteries? *Phys. Chem. Chem. Phys.* **2014**, *16*, 12341−12349.

(25) Preishuber-Pflügl, F.; Bottke, P.; Pregartner, V.; Bitschnau, B.; Wilkening, M. Correlated fluorine diffusion and ionic conduction in the nanocrystalline F^- solid electrolyte $Ba_{0.6}La_{0.4}F_{2.4}$ − ^{19}F $T_{1\rho}$ NMR relaxation vs. conductivity measurements. *Phys. Chem. Chem. Phys.* **2014**, *16*, 9580−9590.

(26) Wiedemann, D.; Nakhal, S.; Rahn, J.; Witt, E.; Islam, M. M.; Zander, S.; Heitjans, P.; Schmidt, H.; Bredow, T.; Wilkening, M.; et al. Unravelling Ultraslow Lithium-Ion Diffusion in γ-$LiAlO_2$: Experiments with Tracers, Neutrons, and Charge Carriers. *Chem. Mater.* **2016**, *28*, 915−924.

(27) Uitz, M.; Epp, V.; Bottke, P.; Wilkening, M. Ion Dynamics in Solid Electrolytes for Lithium Batteries. *J. Electroceram.* **2017**, *38*, 142−156.

(28) Martin, D. Z. C.; Haworth, A. R.; Schmidt, W. L.; Baker, P. J.; Boston, R.; Johnston, K. E.; Reeves-McLaren, N. Evaluating Lithium Diffusion Mechanisms in the Complex Spinel $Li_2NiGe_3O_8$. *Phys. Chem. Chem. Phys.* **2019**, *21*, 23111−23118.

(29) McClelland, I.; Johnston, B.; Baker, P. J.; Amores, M.; Cussen, E. J.; Corr, S. A. Muon Spectroscopy for Investigating Diffusion in Energy Storage Materials. *Annu. Rev. Mater. Res.* **2020**, *50*, 371−393.

(30) Johnston, B. I. J.; Baker, P. J.; Cussen, S. A. Ion Dynamics in Fluoride-Containing Polyatomic Anion Cathodes by Muon Spectroscopy. *J. Phys.: Mater.* **2021**, *4*, 044015.

(31) Magerl, A.; Zabel, H.; Anderson, I. S. In-Plane Jump Diffusion of Li in LiC_6. *Phys. Rev. Lett.* **1985**, *55*, 222−225.

(32) Wagemaker, M.; Kearley, G. J.; van Well, A. A.; Mutka, H.; Mulder, F. M. Multiple Li Positions inside Oxygen Octahedra in Lithiated TiO_2 Anatase. *J. Am. Chem. Soc.* **2003**, *125*, 840−848.

(33) Hu, C.-W.; Lee, C.-H.; Wu, P.-J. Study on the Dynamics of a Vanadium Doped $LiFePO_4$ Lithium-Ion Battery Using Quasi-Elastic Neutron Scattering Technique. *J. Chin. Chem. Soc.* **2021**, *68*, 507−511.

(34) Wiedemann, D.; Indris, S.; Meven, M.; Pedersen, B.; Boysen, H.; Uecker, R.; Heitjans, P.; Lerch, M. Single-Crystal Neutron Diffraction on γ-$LiAlO_2$: Structure Determination and Estimation of Lithium Diffusion Pathway. *Z. Kristallogr. - Cryst. Mater.* **2016**, *231*, 189−193.

(35) Wilkening, M.; Heitjans, P. From Micro to Macro: Access to Long-Range Li^+ Diffusion Parameters in Solids via Microscopic ^{6}Li, ^{7}Li Spin-Alignment Echo NMR Spectroscopy. *ChemPhysChem* **2012**, *13*, 53−65.

(36) Böhmer, R.; Jeffrey, K. R.; Vogel, M. Solid-state LiNMR with applications to the translational dynamics in ion conductors. *Prog. Nucl. Magn. Reson. Spectrosc.* **2007**, *50*, 87−174.
(37) Kuhn, A.; Narayanan, S.; Spencer, L.; Goward, G.; Thangadurai, V.; Wilkening, M. Li Self-Diffusion in Garnet-Type $Li_7La_3Zr_2O_{12}$ as Probed Directly by Diffusion-Induced ^7Li Spin-Lattice Relaxation NMR Spectroscopy. *Phys. Rev. B: Condens. Matter Mater. Phys.* **2011**, *83*, 094302.
(38) Epp, V.; Gün, O.; Deiseroth, H. J.; Wilkening, M. Long-Range Li^+ Dynamics in the Lithium Argyrodite Li_7PSe_6 as Probed by Rotating-Frame Spin-Lattice Relaxation NMR. *Phys. Chem. Chem. Phys.* **2013**, *15*, 7123−7132.
(39) Ding, M. S.; Xu, K. Phase Diagram, Conductivity, and Glass Transition of LiTFSI−H_2O Binary Electrolytes. *J. Phys. Chem. C* **2018**, *122*, 16624−16629.
(40) Nowinski, J. L.; Lightfoot, P.; Bruce, P. G. Structure of $LiN(CF_3SO_2)_2$, a Novel Salt for Electrochemistry. *J. Mater. Chem.* **1994**, *4*, 1579−1580.
(41) Adeli, P.; Bazak, J. D.; Park, K. H.; Kochetkov, I.; Huq, A.; Goward, G. R.; Nazar, L. F. Boosting Solid-State Diffusivity and Conductivity in Lithium Superionic Argyrodites by Halide Substitution. *Angew. Chem., Int. Ed.* **2019**, *58*, 8681−8686.
(42) Heitjans, P.; Masoud, M.; Feldhoff, A.; Wilkening, M. NMR and Impedance Studies of Nanocrystalline and Amorphous Ion Conductors: Lithium Niobate as a Model System. *Faraday Discuss.* **2007**, *134*, 67−82.
(43) Matsumoto, K.; Hagiwara, R.; Tamada, O. Coordination Environment around the Lithium Cation in Solid $Li_2(EMIm)(N(SO_2CF_3)_2)_3$ (EMIm = 1-ethyl-3-methylimidazolium): Structural Clue of Ionic Liquid Electrolytes for Lithium Batteries. *Solid State Sci.* **2006**, *8*, 1103−1107.

https://doi.org/10.1021/acsphyschemau.1c00032
ACS Phys. Chem Au 2022, 2, 136−142